



UNIVERSITY OF LEEDS

This is a repository copy of *Investigating the micro mechanics of cemented sand using DEM*.

White Rose Research Online URL for this paper:  
<http://eprints.whiterose.ac.uk/109391/>

Version: Accepted Version

---

**Article:**

de Bono, J, McDowell, G and Wanatowski, D (2015) Investigating the micro mechanics of cemented sand using DEM. *International Journal for Numerical and Analytical Methods in Geomechanics*, 39 (6). pp. 655-675. ISSN 0363-9061

<https://doi.org/10.1002/nag.2340>

---

(c) 2015, Wiley. This is the peer reviewed version of the following article: de Bono, J, McDowell, G and Wanatowski, D (2015) Investigating the micro mechanics of cemented sand using DEM. *International Journal for Numerical and Analytical Methods in Geomechanics*, 39 (6). pp. 655-675, which has been published in final form at <https://dx.doi.org/10.1002/nag.2340>. This article may be used for non-commercial purposes in accordance with Wiley Terms and Conditions for Self-Archiving.

**Reuse**

Items deposited in White Rose Research Online are protected by copyright, with all rights reserved unless indicated otherwise. They may be downloaded and/or printed for private study, or other acts as permitted by national copyright laws. The publisher or other rights holders may allow further reproduction and re-use of the full text version. This is indicated by the licence information on the White Rose Research Online record for the item.

**Takedown**

If you consider content in White Rose Research Online to be in breach of UK law, please notify us by emailing [eprints@whiterose.ac.uk](mailto:eprints@whiterose.ac.uk) including the URL of the record and the reason for the withdrawal request.



[eprints@whiterose.ac.uk](mailto:eprints@whiterose.ac.uk)  
<https://eprints.whiterose.ac.uk/>

# INVESTIGATING THE MICRO MECHANICS OF CEMENTED SAND USING DEM

John de Bono, Glenn McDowell, Dariusz Wanatowski

## INTRODUCTION

Cemented sand occurs naturally through a number of processes, and as a result samples exhibit a high variation in density and degree of cementation (Airey, 1993). There are also difficulties involved in extracting natural specimens while avoiding disturbance. Soils are also artificially cemented, primarily to improve performance, and are commonly used in pavement subbase layers. Leroueil and Vaughan (1990) used the term 'structured soils' to comprise cemented sands, over-consolidated clays, and weak rocks, and showed that they follow the same principal behaviour and that the physical properties of the cemented soil govern its behaviour, rather than the cause of cementation. Hence it has been convenient to perform tests on artificially cemented sands to draw conclusions and deepen understanding, for example Clough et al. (1981), Coop and Atkinson (1993), Haeri et al. (2004).

The majority of published research on cemented sand under triaxial conditions is at conventional pressures (typically under 1MPa). Coop and Atkinson (1993) demonstrated that the addition of a cementitious material to sand introduces well defined yield points (identified from the discontinuity of the initial stress-strain curve, and onset of plastic volumetric strains) into the stress-strain response during triaxial shearing, which can be related to the breakage of cementation. At large axial strains, both cemented and uncemented sands reached steady conditions, i.e. critical state, and notably appeared to have the same critical state line. They outline three modes of failure for cemented soils, defined by when yielding (breakage) of the bonding occurs. The first case is when cement bonds break during isotropic consolidation, causing subsequent shearing behaviour similar to that of the equivalent uncemented soil. The second case is where bonds are initially intact but break during shearing, and any peak state is governed by the frictional properties of the equivalent non-structured soil. Thirdly, when the bonds yield after shearing has commenced, this causes a clear peak stress to occur.

The discrete element method (DEM) has proved a useful tool for modelling granular material. DEM uses two entities: a ball and a wall to model interactions and Newton's 2<sup>nd</sup> Law together with a contact law to establish the accelerations, velocities and displacements of particles via a time-stepping scheme. The most commonly used DEM software in use is PFC3D (Itasca, 2005), which is the software used by the authors to simulate cemented and uncemented sand under high-pressure triaxial conditions. The principal variables investigated are the numerical bond properties, cement content, and high confining pressures.

## TRIAXIAL BEHAVIOUR OF CEMENTED SAND

### Conventional Pressures

At low confining pressures, Huang and Airey (1998) showed that cementation causes an increase in stiffness, peak strength, maximum rate of dilation, and in general the specimen becomes more brittle. These effects all increase with increasing cement content. At higher confining pressures, the

cementation appears broken down and the normalised stress-strain responses for various cement contents appear identical. Schnaid et al. (2001) performed a series of drained triaxial tests on cemented sand at low pressures and demonstrated how significantly the soil behaviour is influenced by cement content. They also observed an initial volumetric contraction followed immediately by a significant dilation, before a steady state was reached, with the highest cement contents exhibiting the most dilation. The maximum rate of dilation was found to occur just after the peak strength, which is dissimilar to uncemented materials – for which the maximum dilation rate coincides with peak deviatoric stress. Similar behaviour has been reported by Asghari et al. (2003) and Haeri et al. (2004) who also categorised failure modes: brittle failure with shear planes for cemented samples and barrelling failure for equivalent uncemented samples. An increase in confining pressure suppresses the effects of cementation and causes a transition from brittle to ductile behaviour. It also increases the maximum deviatoric stress, although the axial strain associated with this stress decreases with increasing cement content.

### **High Pressure**

Consolidated drained triaxial tests have been performed on specimens with Portland cement contents from 0-15% dry weight by Marri et al. (2012), across confining pressures of 1, 4, 8 and 12MPa. Selected results are displayed in Figure 1.

The addition of cement causes an increase in peak deviatoric stress, a reduction in the strain associated with this stress, and an increase in dilation. An increasing amount of cement causes the behaviour to become more brittle.

Marri et al. (2012) showed that uncemented specimens exhibit strain hardening with no peak deviatoric stress, and undergo contraction during shearing, demonstrating completely ductile behaviour, while the addition of cement causes a peak stress to occur, with the peak stress increasing and becoming more distinguished with higher cement content. This is consistent with previous work on artificially cemented and uncemented sands at low pressures (e.g. Abdulla and Kiousis, 1997), Marri et. al. (2012) also showed that with increasing cement content, the axial strain associated with the peak reduces, and the initial modulus of deformation becomes higher, and causes an increase in both the amount and rate of dilation.

For a given confining pressure, both uncemented and cemented specimens deviatoric stress responses appear to converge or be approaching convergence after large strains, due to the cemented specimens becoming 'destructured' and behaving almost as uncemented. However, they often do not quite converge, especially at high cement contents, due to a portion of bonds remaining intact, causing groups of particles to behave as larger particles, effectively changing the grading.

Confining pressure has equally important effects on the behaviour of cemented sand; high pressures suppress the effects of cementation, and render the behaviour from brittle to ductile. Increasing confining pressure causes higher maximum deviatoric stress, and reduces dilation. At the highest pressures, no clear peak stress is apparent, with specimens displaying ductile behaviour, with a gradually increasing deviatoric stress approaching a steady maximum value. The specimens also

undergo contraction, in contrast to those sheared at lower pressures. However, the effects of cementation can still be observed at higher pressures when compared with the uncemented material.

At intermediate confining pressures, such as 4 and 8MPa, the behaviour is neither completely brittle nor ductile. The cemented samples at 1MPa demonstrate brittle behaviour, with clear peak states with strain softening, and shear planes visible in the highly cemented samples (Figure 1a). At 12MPa, all cemented samples demonstrate ductile failure, with gradual strain hardening and volumetric contraction, and barrelling failure modes visible. From lower to higher confining pressures there is a general transition from brittle to ductile behaviour.

## **DISCRETE ELEMENT METHOD**

### **Triaxial Model**

The triaxial model used in this work is the same as outlined in de Bono et al. (2012), which features a flexible membrane that allows the true failure mode to develop while maintaining a constant confining pressure. The model is capable of applying high confining pressures to the specimen. The membrane consists of bonded particles a factor of 0.66 smaller than the smallest specimen particle; the properties are listed in **Table 1**.

The sample used herein has a height of 100mm and a radius of 50mm. The sand grains are represented by spherical particles, generated using the radii expansion method (Itasca, 2005). The numerical sample requires the user to specify 3 parameters: voids ratio, coefficient of uniformity ( $C_u = D_{60}/D_{10}$ ) and the minimum sample particle diameter ( $D_{min}$ ). The sample is continuously graded, with the simplified grading curve obtained from the coefficient of uniformity ( $C_u$ ), similar to the method described by Potyondy and Cundall (2004). A value of  $C_u=2$  is used, approximately that of Portaway Sand, the base soil used by Marri et al. (2012). Thus for a given voids ratio and grading, the specified minimum diameter,  $d_{min}$  directly determines how many particles are generated. The size of the smallest particle controls the numerical timestep as well as the total number of particles which in turn influences the calculation time. Varying  $d_{min}$  does not necessarily change the packing geometry; it shifts the position of the grading curve.

Wang & Leung (2006) suggested using a normal particle stiffness of the order  $10 \cdot 10^6 \text{N/m}$  for quartz sand, and also that the same value can be used for both normal and shear stiffness. In the simulations presented, the sand particles were given a normal stiffness of  $10 \cdot 10^6 \text{N/m}$ , and to reduce the number of input parameters particle shear stiffness was also assigned this value. Density was set at  $2650 \text{kg/m}^3$ , reflecting the density of the sand used in the aforementioned laboratory experiments (Marri et al. 2012), and a particle friction value of 0.5 was attributed. The specimens were created in a dense initial state, with an initial voids ratio of 0.55, consisting of 6759 particles.

### **Inter-Particle Bonding**

Cement bonds are modelling using 'Parallel Bonds', a feature of the software (Itasca 2005). These consist of a finite-sized cylindrical piece of material between the two particles, which acts in parallel with the standard force-displacement contact model. These have been used in previous studies, e.g.

Potyondy and Cundall (2004) and Wang and Leung (2006). The bonds are defined by normal and shear stiffness (in terms of stress/displacement), normal and shear strength (in terms of stress) and bond size per unit area of the bond.

With regards to the literature, it is somewhat unclear how to simulate the size of cement bonds. One might consider them as small relative to the particles, occurring just at the contacts and independent of particle size, or alternatively to consider them as proportional to the particles, filling much of the void space. Both of these approaches seem justifiable depending on interpretation of the nature of cementation and analysis of images. In this study, in order to isolate and investigate bond strength distributions, all bonds are created with equal size (radius equal to the smallest sand particle), therefore having equal moment resistance. To reduce the number of variables, and because this study is not exclusively concerned with calibration against physical tests, parallel bond stiffnesses have been defined to give values equal to the particle stiffnesses (in terms of force/displacement).

Bonds are installed at existing inter-particle contacts. For a dense arrangement of particles, with the parameters described above, this method installs approximately 5 bonds per particle, and leaves a small number (4%) of free particles with no bonds. A series of simulations have been conducted to investigate solely the bond strength distributions, using a triaxial sample with approximately 17,000 parallel bonds (each particle has an average of 5 neighbouring particles bonded to it). Considering that the numerical sample has an approximately equal coefficient of uniformity and density to the material from results shown in Figure 1, this configuration of bonds can be considered analogous to a given material, i.e. Portaway sand with 5% cement content.

The principal effects of the parallel bonds are evident in Figure 2 where the deviatoric stress versus axial strain responses are shown from simulations of three cemented materials along with an uncemented sample, sheared under a confining pressure of 1MPa. The cemented samples have completely uniform bonds, i.e. there is no strength distribution. All bonds are equal in size, stiffness and strength in each test, with only the bond strength varied across the three simulations.

The three different parallel bond strengths have been defined as 7.96, 15.92 and 31.83 N/mm<sup>2</sup>, to give strengths of 25, 50 and 100N respectively in pure shear and tension. It is immediately evident that the introduction of cement bonds with strengths 50 and 100N cause a large peak deviatoric stress to appear and increases the maximum stress compared to the unbonded sample. The simulation with bonds of strength 25N has a smaller peak stress, with almost all the bonds breaking soon upon commencement of shearing, after which behaviour similar to the uncemented sample is observed. The peak stress witnessed in the cemented simulations is caused by the presence of bonds, with the peak appearing to coincide with the onset of major bond breakage (Figure 2c). All bonded samples exhibit a stiffer initial response compared to the unbounded equivalent. The cemented samples approach the stress state of the uncemented simulation as the bonds eventually become broken down, and the material becomes destructured. Inspecting the graphs of volumetric strain versus axial strain shows that the most strongly bonded sample undergoes slightly more dilation than the other simulations (Figure 2b).

The bond uniformity is reflected in the graphs; the very sharp peak indicates extremely brittle failure and rapid onset of bond breakage. It is apparent from the graph that there is an initial linear region, during which no bonds have broken, particularly for the 100N bond strength. This seems somewhat

unrealistic, especially at these stress levels. It is evident from the literature (e.g. Airey, 1993; Asghari et al., 2003) that one might expect such a sharp peak with an initially linear response at very low pressures (typically under 100kPa), however as is visible in Figure 1, no sharp peaks or such brittle behaviour is witnessed at higher pressures, with only the highest cement content producing a rounded peak. One might therefore assume that a distribution of bond strengths would yield more realistic results, i.e. a more rounded peak stress with gradual bond failure. Figure 3 compares the results of cemented simulations with the same initial setup as the previous, but with parallel bond strengths satisfying three different probability distributions: uniform, normal and Weibull.

Figure 3(a) and (b) show the deviatoric stress response of samples with bond strengths satisfying two alternative uniform distributions and two normal distributions, all with the same mean strength of 50N. The bonds with uniformly distributed strengths have ranges of 50 and 100N, and the normally distributed bonds have coefficient of variations of 0.2 and 0.4. Also included is the response of the simulation with completely uniform bonds with unique strength of 50N, as well as the unbonded simulation.

It can be seen that the samples with uniformly distributed bond strengths show lower maximum stresses, with the peaks more rounded. The sample with bond strengths ranging from 0-100N experiences bond breakage immediately, and as such has the lowest and most rounded peak deviatoric stress. The simulation with the narrower range, i.e. bond strengths ranging from 25-75N has a finite minimum bond strength, so there will be an initial linear region during which no bond breakage is witnessed.

The samples with normal bond strength distributions give similar stress-strain results, despite exhibiting slightly different bond breakage. The simulation with the smaller coefficient of variation behaves very similarly to the sample with no strength distribution, while the sample with the larger coefficient displays an earlier, less sudden onset of breakage. However, both the simulations with uniform and normal bond strength distributions still display sharp distinct peak stresses, indicating sudden failure due to most bond strengths lying close to the mean value. All of these simulations display approximately the same volumetric strain during shearing.

Figure 3(c) shows the results from 3 simulations with bond strengths from Weibull distributions, all with the same mean value but with differing distribution parameters. A Weibull distribution is defined by two variables, denoted in this paper as the modulus,  $m$ , and the scale parameter,  $\lambda$ . The modulus determines the shape of the distribution; the scale parameter determines the size/range. The mean of a Weibull distribution is given by:

$$\mu = \lambda \Gamma(1 + 1/m)$$

and so is affected by both parameters ( $\Gamma$  is the gamma function). Changing the modulus (shape) of a Weibull distribution slightly alters the mean, so the scale of the distribution needs to be adjusted to maintain the same mean. For a given scale,  $\lambda$ , increasing the modulus results in a narrower distribution. Weibull probability is used widely in materials science, especially in failure probability of brittle materials, so it seems reasonable that such a distribution of may be applicable to cementation. It has also been used in the field of geomechanics, in particular particle breakage, for example McDowell & Amon (2000), and McDowell (2001).

Examining the results of the various Weibull distributions of bond strengths reveals that the lower the modulus, the more rounded the peak stress. Higher values of  $m$  render the distribution and behaviour of the bonded sample similar to that with normally distributed strengths. Lower values of  $m$ , i.e. less than or equal to 1 produce a positively skewed, very wide distribution of strengths. It can be seen that the sample with a modulus of 0.5 produces a rounded peak stress, which appears the most similar to the experimental stress-stress curves at high pressures shown in Figure 1(a). This indicates a much less sudden onset of bond breakage, which is also apparent from the graph displaying the number of intact bonds versus axial strain. Although a significant number of bonds are broken during consolidation, the maximum rate of breakage during shearing is slightly lower. The full triaxial results for these simulations are shown in Figure 4, which also shows the volumetric strain versus axial strain, and the number of intact bonds versus strain. The simulation with the lowest  $m$  value demonstrates the most dilation and also the fewest remaining bonds for a given axial strain, a different trend to that in Figure 2, where the greatest dilation is associated with the largest number of intact bonds after shearing. This suggests that for the simulation with a Weibull modulus of 0.5, although fewest bonds remain, the bonds that do remain heavily influence the behaviour. For the simulation with  $m=0.5$ , after shearing (20% axial strain) the remaining bonds (approximately 2000) have a mean strength of 256N covering a range of 2992N. In contrast, the simulation with  $m=2.0$  has approximately 4200 bonds remaining with a mean strength of 63N covering a range of 158N.

Figure 5 shows histograms for the bond strength distributions for the three simulations with Weibull moduli 0.5, 1.0 and 2.0, before and after shearing. Figure 5(a) shows the three histograms before consolidation, therefore before any bonds have broken. Most bonds in the simulation with  $m=0.5$  have strengths between 0 and 40N, whereas in the simulation with  $m=2.0$ , most bond strengths lie around the mean value of 50N. Figure 5(b) shows histograms plotting the residual bond strengths after shearing to 20% axial strain, in which the difference in the quantity of remaining bonds can also be observed. While the simulation with  $m=2.0$  (narrower distribution of strengths) has a greater number of unbroken bonds remaining, the remaining bonds in the simulation with  $m=0.5$  are significantly stronger – almost all of the weaker bonds have yielded. This suggests that it is the strength of the strongest bonds that most influence the behaviour.

Inspecting the sheared samples reveals contrasting patterns of breakage; the simulation with the wider range of bond strengths ( $m=0.5$ ) shows intact bonds distributed throughout the height of the sample, while the opposing specimen with  $m=2.0$  displays localised bond breakage, with most of the remaining intact bonds located close to the platens (Figure 6). During shearing, it tends to be the particles in the middle of a given specimen that will undergo the most displacement, and the images suggest that for the sample with a narrow range of bond strengths ( $m=2.0$ ), the bonds offer little resistance to this deformation, with almost no bonds remaining around the middle. For the sample with the much wider distribution ( $m=0.5$ ), fewer total bonds remain unbroken however there are still bonds distributed throughout the height of the sample, which offer most resistance to shear deformation, hence the higher dilation. Groups of particles bonded together in 'clusters' exist, which behave as larger, irregular shaped particles, effectively changing the grading – similar to laboratory observations mentioned previously.

## **Cement Content**

Potentially, there are numerous ways one might simulate a range of cement contents. Analysis of experimental data could suggest altering the variation or magnitude of bond strengths and stiffness, or various combinations thereof, while analysing the images in Figure 7 would suggest altering the quantity of bonds and/or bond size.

The effects of increasing the magnitude of bond strength have been shown previously in Figure 2. While there is an increase in peak strength, there is little effect on the volumetric behaviour, and increasing the bond strength increases the strain at which the peak occurs, contrary to real behaviour. If the bond stiffness alone is increased, this causes a decrease in the axial strain to the peak strength, however both the peak stress and amount of dilation are decreased due to bonds breaking earlier and therefore fewer remain to resist deformation. If larger bonds are installed, the correct increase in dilation is observed, however there is very little change in the peak strength, and no effect on the specimen's initial stiffness.

If one considers the quantity of bonds, it appears common practise when modelling bonded granular materials to install bonds at existing inter-particle contacts (e.g. Potyondy and Cundall, 2004; Wang and Leung, 2006). For the dense sample described above, this method installs approximately 5 bonds per particle and leaves a small number of free unbonded particles. Visually inspecting SEM images of cemented sand, such as those in Figure 7 evidently suggests a greater number of bonds are required to accurately represent varying levels of cementation. The cement can be seen to fill voids and connect particles which otherwise would not be in contact. Inspecting Figure 7(a), which shows a specimen with 5% cement content, a typical sand particle visibly has 5 or 6 surrounding particles bonded to it, whereas a sand particle in the specimen with 15% cement content appears to have typically more - as many as 9 bonded to it which are visible. Bearing in the mind the planar nature of the images, one could expect a particle not on the surface of a cemented specimen to have an even greater number of surrounding particles bonded to it.

Using the bond parameters which give the most realistic stress behaviour (i.e. Weibull strength distribution with  $m=0.5$  and mean strength 50N), a series of triaxial simulations have been performed with an increasing number of bonds. Considering the quantity of bonds (in this paper measured by the average number of bonds per sand particle) as a gauge of cement content, results are presented for simulations with an average of 5, 10 and 20 parallel bonds per sand particle, alongside an unbonded simulation. All simulations are sheared under a confining pressure of 1MPa. The increased number of bonds is achieved by bonding particles which aren't necessarily touching, but which lie within a specified proximity of one another. Adjusting this proximity results in a larger or smaller number of bonds among the sand particles.

From Figure 8, it can be seen that the correct qualitative behaviour with regards to modelling increased cement content is reproduced by increasing the number of bonds. There is an increase in the peak and maximum deviatoric stress, a higher initial stiffness, and there is a more dilative volumetric response. The peak stress appears at approximately the same axial strain regardless of the number of bonds. The stress-strain responses appear to converge at large strains. Considering the increasing number of bonds to be equivalent to 5, 10 and 15% cement contents respectively, the results demonstrate good qualitative agreement with the results in Figure 1(a). Increasing the number of bonds produces the correct transition from ductile to brittle behaviour. The difference in failure modes is most visible in Figure 9 which displays the particle rotations at approximately the

point of maximum rate of dilation (2-3% axial strain). The lightly bonded sample displays no clear pattern, and exhibits classic barrelling failure, while the heavily bonded sample displays a clear shear plane, typical of a highly cemented, brittle material.

### **Confining Pressures**

Again, using the bond parameters which give the most realistic stress behaviour (i.e. Weibull distribution with  $m=0.5$  and mean strength 50N) triaxial simulations have been performed over a range of high confining pressures (1MPa – 12MPa). Assuming that the average number of bonds per particle is representative of a given cement content, Figure 10 shows the effects increasing the confining pressure has on the behaviour of cemented sand, with the behaviour of a sample with an average of 10 bonds per particle (considered a medium cement content, such as 10%) plotted for confining pressures of 1, 4, 8 and 12MPa.

It is clear from the graph that increasing the confining pressure leads to a higher maximum deviatoric stress. The graph is comparable with experimental results shown in Figure 1(b). The strain associated with the maximum deviatoric stress increases with confining pressure. The peak is much more prominent at lower pressures, becoming less distinguished at 12MPa. As with experimental results, there is a transition from brittle to ductile behaviour, with the effects of cementation/bonds being suppressed by increasing confinement.

Confining pressure also greatly reduces the volumetric dilation, with the sample becoming more contractive with increased confining pressure. It can be seen that the axial strain associated with the maximum rate of dilation increases with increasing confining pressure, in the same manner as the experimental results shown in Figure 1(b). However, the correct magnitude of contraction is impossible to attain in the simulations without taking particle crushing into consideration. This also is the reason why there exists a peak in the deviatoric stress graphs, even at pressures as high as 12MPa.

The change in failure behaviour from brittle to ductile is visible in the sheared samples: **Figure 11** plots the particle rotations at approximately the maximum rate of dilation (2 and 6% axial strain respectively for the samples sheared at 1 and 12MPa confining pressures). Conjugate shear bands are visible in the simulation at 1MPa confining pressure, while no distinct pattern is visible at 12MPa. **Figure 12** shows the final numerical specimens after 20% axial strain, alongside the equivalent laboratory samples (contrasting confining pressures of 1 and 12MPa). From the images of the real specimens after shearing, conjugate shear planes can be observed through the membrane for the sample with 10% cement content sheared at 1MPa. Similar failure can be seen in the corresponding image of the numerical sample, which has fairly distinctive non-uniform deformations. The same material shearing under a confining pressure of 12MPa displays barrelling failure, i.e. expansion which is uniform in the radial direction, and concentrated around the mid height of the specimen.

### **CONCLUSIONS**

A series of DEM simulations of high pressure triaxial tests have been performed on cemented and uncemented materials. The cementation has been modelled with parallel bonds, and a variety of bond strength distributions have been investigated. For a given mean bond strength, a Weibull distribution with a modulus of 0.5 appears to give the most realistic results; with some bonds failing during consolidation and immediately after commencing shearing, while the strongest remain intact throughout the tests. Such a distribution produces a sharp peak strength at lower confining pressures, and a more rounded peak at the highest pressures. The presence of bonds, which represent cementation, also cause additional dilation when compared to the uncemented simulations. Increasing the quantity of bonds in a given sample appears to be the most effective way of modelling increased cemented content. For a given distribution of bond strengths, increasing the quantity, by bonding particles to neighbouring ones which aren't in contact but lie within a specified proximity, results in the correct qualitative change in behaviour that an increase in cement content causes in laboratory triaxial tests. It causes a more clearly defined peak strength, an increase in strength/maximum deviatoric stress, increases the dilation, and renders the behaviour more brittle. The flexible membrane used in this study allows the correct failure modes to develop, and contrasting brittle and ductile failure modes have been observed in the specimens after shearing. By plotting the individual particle rotations, it has been shown that for a given confining pressure such as 1MPa, increasing the number of bonds (i.e. the virtual cement content) increases the strength and brittleness of the material, with shear planes produced in the most highly cemented simulations. For a given cement content, increasing the confining pressure to 12MPa suppresses the behaviour of the cementation, with no shear planes visible for even the most highly cemented samples. In between these pressures there is 'transitional' behaviour, where the material behaves neither completely brittle nor ductile. DEM has therefore been shown to be able to capture the behaviour of cemented sand under a range of confining pressures and cement contents.

Future work incorporating particle crushing into the model needs to be undertaken to enable realistic magnitudes of volumetric contraction to be observed. This will most likely also have an effect on the stress response, especially if a distribution of particle strengths is used. Investigating the coupled effects of particle strength distributions and bond strength distributions will provide valuable insight into the micro-mechanics of cemented sand at high pressures, and is a necessary step before any calibration can be made with laboratory tests.

## REFERENCES

- Abdulla, A. A., & Kiousis, P. (1997). Behavior of cemented sands-I. Testing. *Int. J. Numer. Anal. Meth. Geomech.* , 21, 533-547.
- Airey, D. (1993). Triaxial Testing of Naturally Cemented Carbonate Soil. *Journal of Geotechnical Engineering* , 119 (9), 1379-1398.
- Asghari, E., Toll, D., & Haeri, S. (2003). Triaxial Behaviour of a Cemented Gravelly Sand. *Geotechnical and Geological Engineering* , 21, 1-28.
- Clough, G., Sitar, N., Bachus, R., & Rad, N. (1981). Cemented Sands under Static Loading. *Journal of Geotechnical Engineering* , 107, 799-818.
- Coop, M., & Atkinson, J. (1993). The Mechanics of Cemented Carbonate Sands. *Geotechnique* , 43 (1), 53-68.
- de Bono, J., McDowell, G., & Wanatowski, D. (2012). Discrete element modelling of a flexible membrane for triaxial testing of granular material at high pressures. *Geotechnique Letters* , 2 (4), 199-203.
- Haeri, S., Hamidi, A., & Tabatabaee, N. (2004). The Effect of Gypsum Cementation on the Mechanical Behaviour of Gravelly Sands. *Geotechnical Testing Journal* , 28 (IV).
- Huang, J., & Airey, D. (1998). Properties of Artificially Cemented Carbonate Sand. *Journal of Geotechnical and Geoenvironmental Engineering* , 124 (6), 492-499.
- Itasca. (2005). *Particle Flow Code in Three Dimensions, Software Manual*. Minnesota, MN: Itasca Consulting Group Inc.
- Leroueil, S., & Vaughan, P. (1990). The General and Congruent Effects of Structure in Natural Soils and Weak Rocks. *Geotechnique* , 40 (3), 467-488.
- Marri, A., Wanatowski, D., & Yu, H. (2012). Drained behaviour of cemented sand in high pressure triaxial compression test. *Geomechanics and Geoengineering: An International Journal* , DOI:10.1080/17486025.2012.663938.
- McDowell, G. R., & Amon, A. (2000). The application of Weibull Statistics to the fracture of soil particles. *Soils and Foundations* , 40 (5), 133-141.
- McDowell, G. (2001). Statistics of Soil Particle Strength. *Geotechnique* , 51 (10), 897-900.
- Potyondy, D., & Cundall, P. (2004). A Bonded-Particle Model for Rock. *International Journal of Rock Mechanics & Mining Sciences* (41), 1329-1364.
- Schnaid, F., Prietto, P., & Consoli, N. (2001). Characterization of Cemented Sand in Triaxial Compression. *Journal of Geotechnical and Geoenvironmental Engineering* , 127 (10), 857-868.
- Wang, Y., & Leung, S. (2006). A Particulate-Scale Investigation of Cemented Sand Behaviour. *Canadian Geotechnical Journal* , 45, 29-44.

## FIGURES

<b>Sample Properties</b>	
Size (mm)	50 x 100
No. of Particles	6759
Friction coefficient	0.5
Normal and shear stiffness (N/m)	$10 \times 10^6$
Density ( $\text{kg/m}^3$ )	2650
Coefficient of uniformity	2.0
Minimum particle diameter (mm)	2.0
Median particle size (mm)	4.0
Initial voids ratio	0.55
Contact model	Linear springs (default)
Damping coefficient	0.7 (default value)
Bond diameter (mm)	2
Mean bond normal and shear strength ( $\text{N/mm}^2$ )	15.92*
Mean equivalent bond strength in pure tension and pure shear (N)	50*
<b>Membrane Properties</b>	
No. of particles	11979
Friction coefficient	0.0
Normal and shear stiffness (N/m)	$0.6 \times 10^6$
Density	1000
Particle size (mm)	0.67

\*unless stated otherwise

**Table 1. Summary of DEM properties of the sample and membrane**

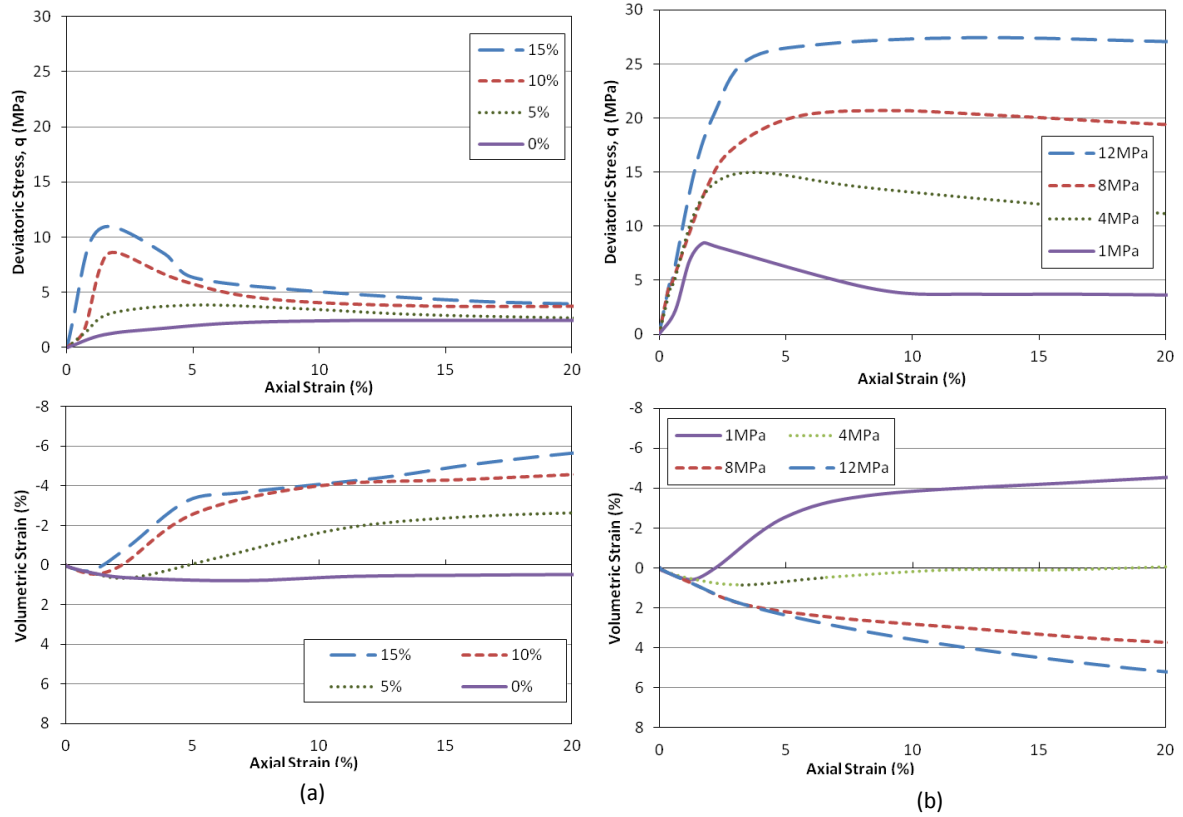


Figure 1. Stress-strain behaviour of various cement contents under (a) 1MPa confining pressure, and (b) 5% cement content sheared under a range of high confining pressures

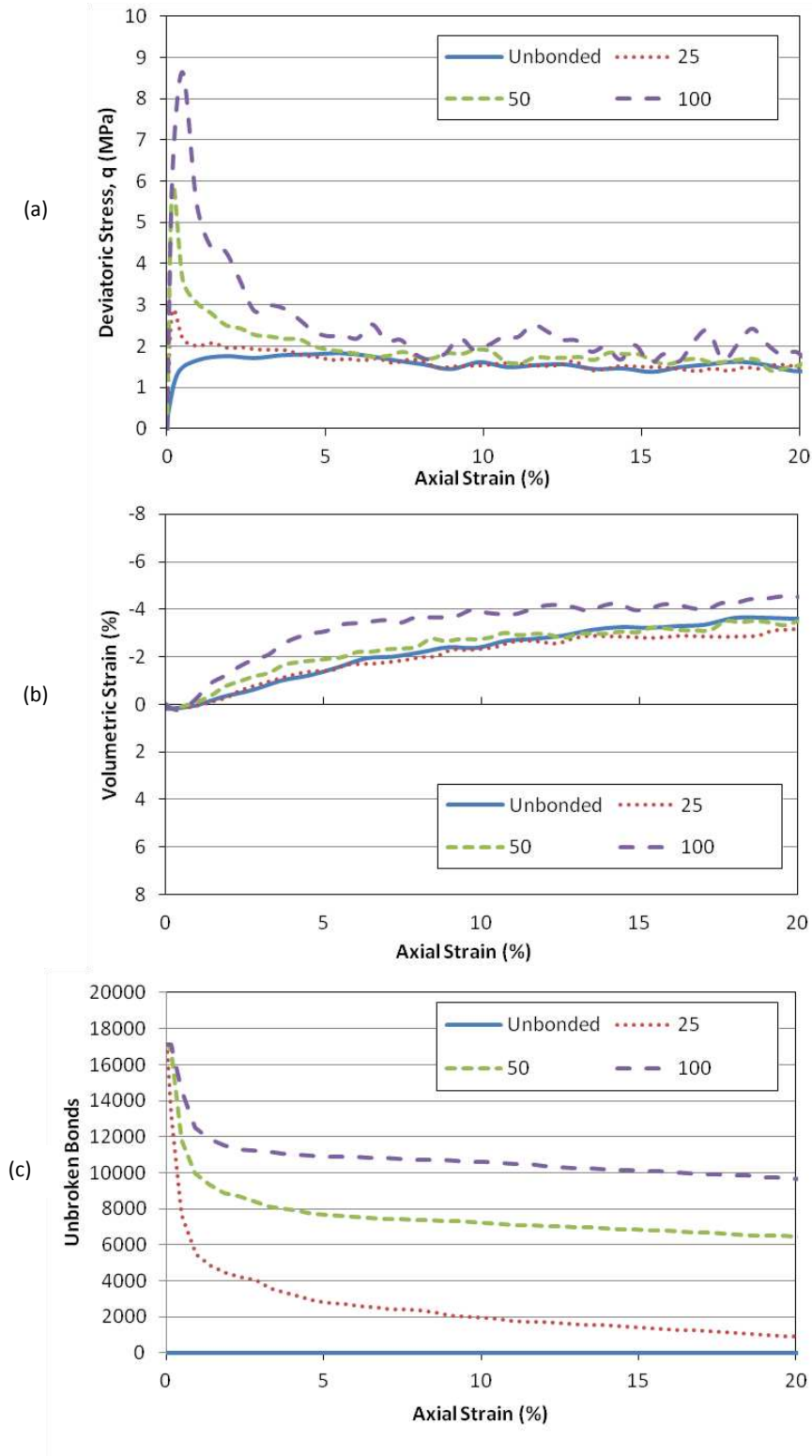


Figure 2. Stress-strain behaviour of simulations with various bond strengths: deviatoric stress (a), volumetric strain (b) and unbroken bonds (c) versus axial strain

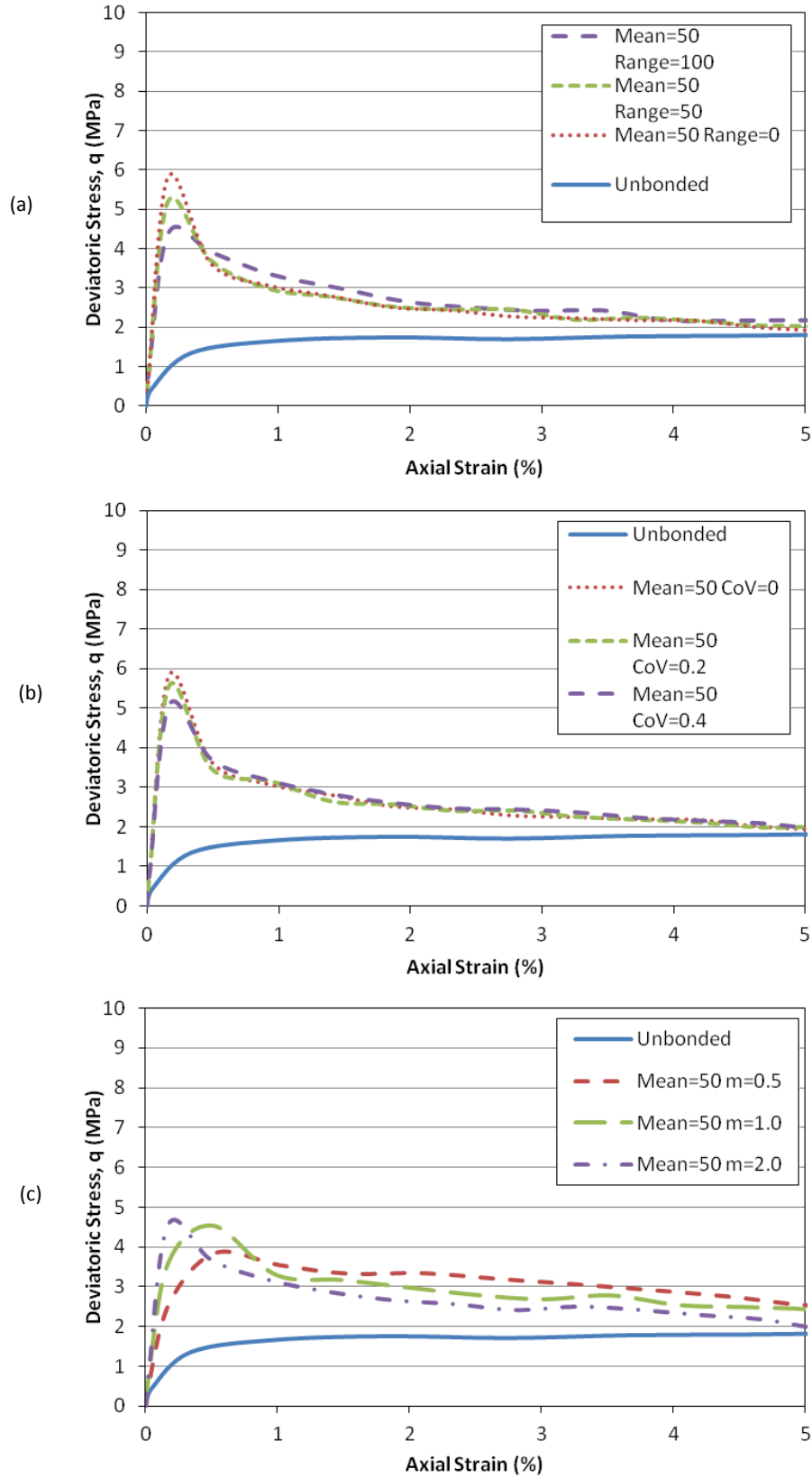


Figure 3. Deviatoric stress versus axial strain for simulations with various uniform (a), normal (b) and Weibull (c) bond strength distributions, with mean strength of 50N

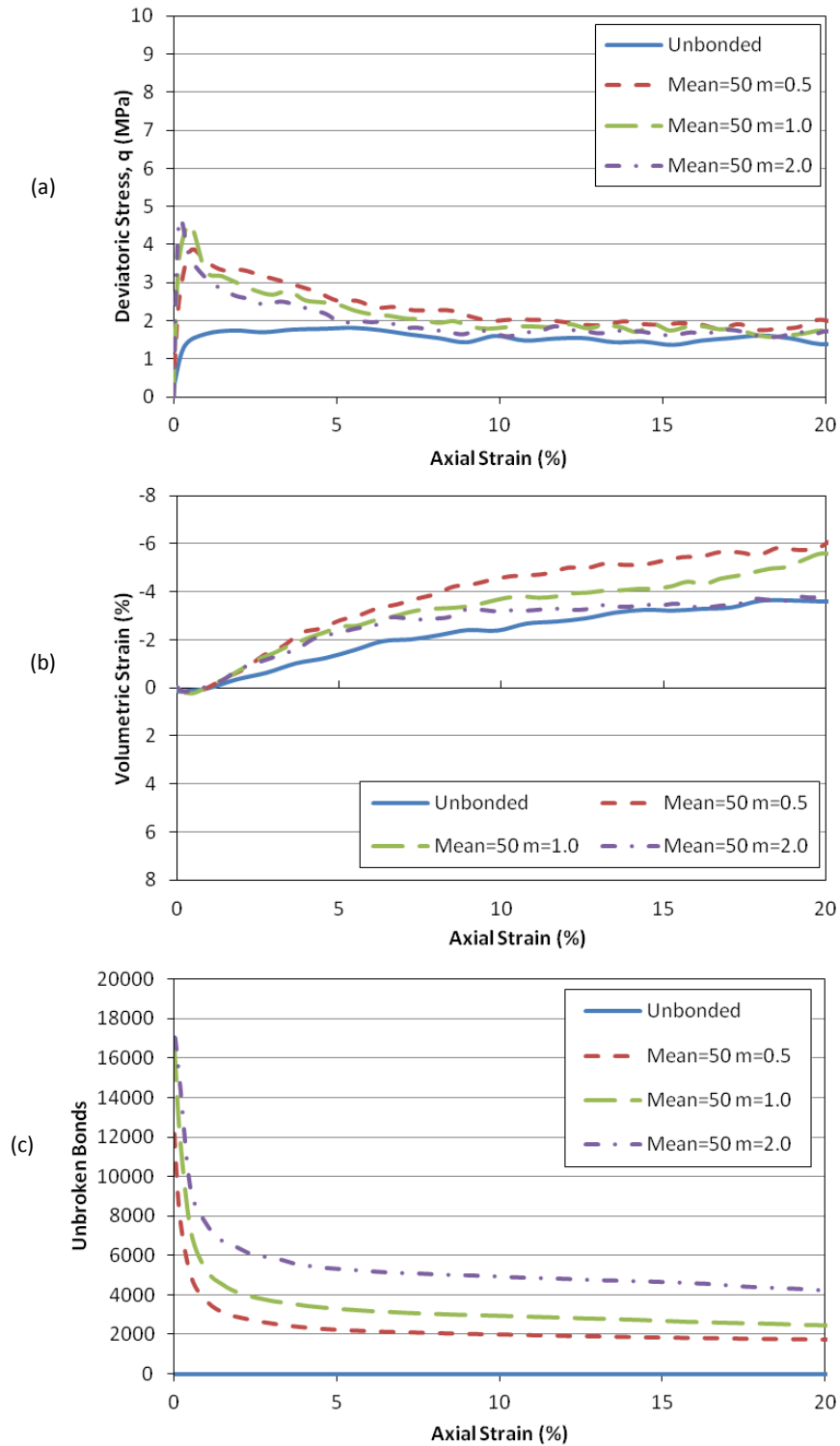


Figure 4. Triaxial behaviour of simulations with Weibull bond strength distributions with various  $m$  values: deviatoric stress (a), volumetric strain (b) and remaining unbroken bonds (c) versus axial strain

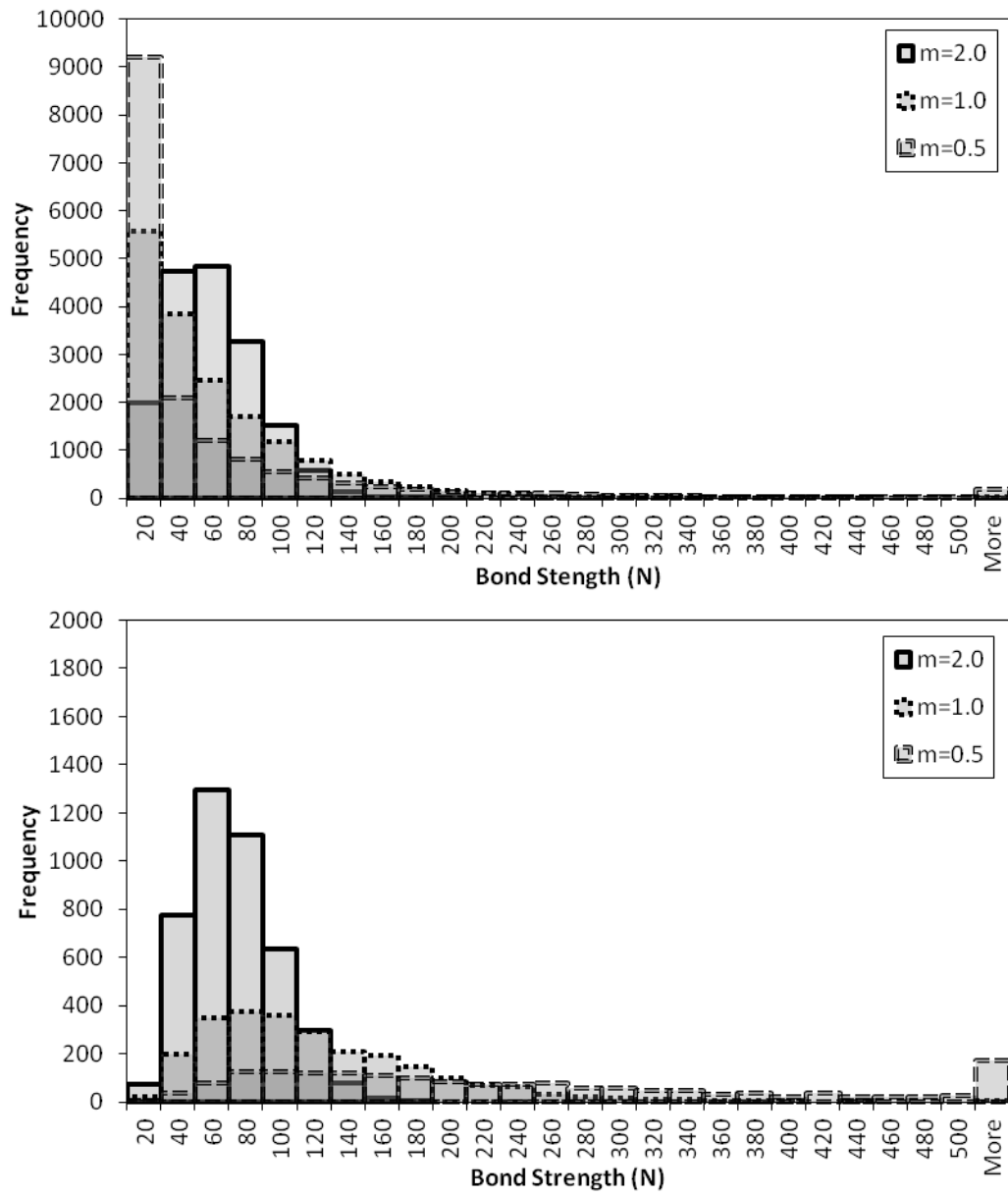


Figure 5. Histograms showing the character of bond strength distributions before (a) and after (b) triaxial shearing

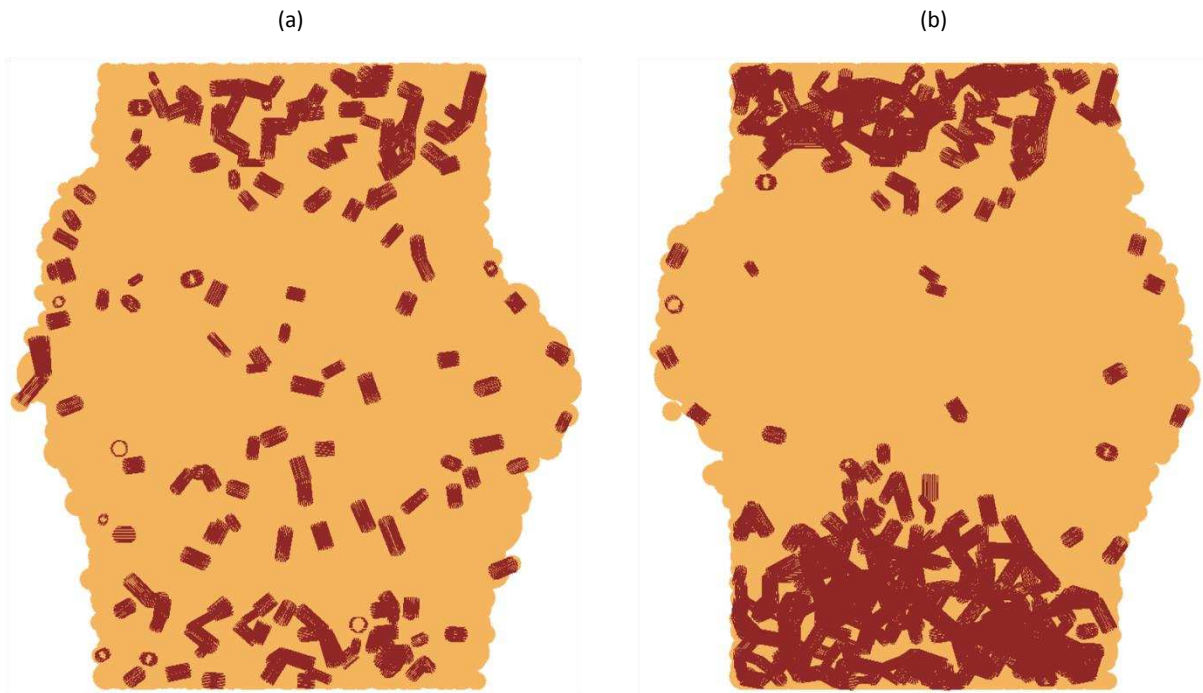


Figure 6. Diagrams showing remaining unbroken bonds on a cross-sectional plane through the sample after 20% axial strain: sample with Weibull bond distribution with (a)  $m=0.5$  and (b)  $m=2.0$

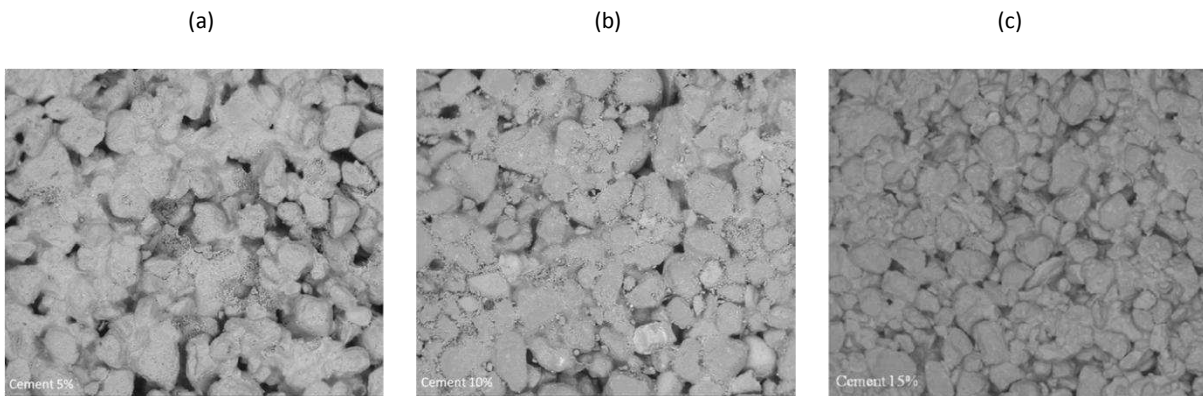


Figure 7. Images of triaxial specimens prepared with various cement contents: (a) 5% ; (b); 10% ; (c) 15%

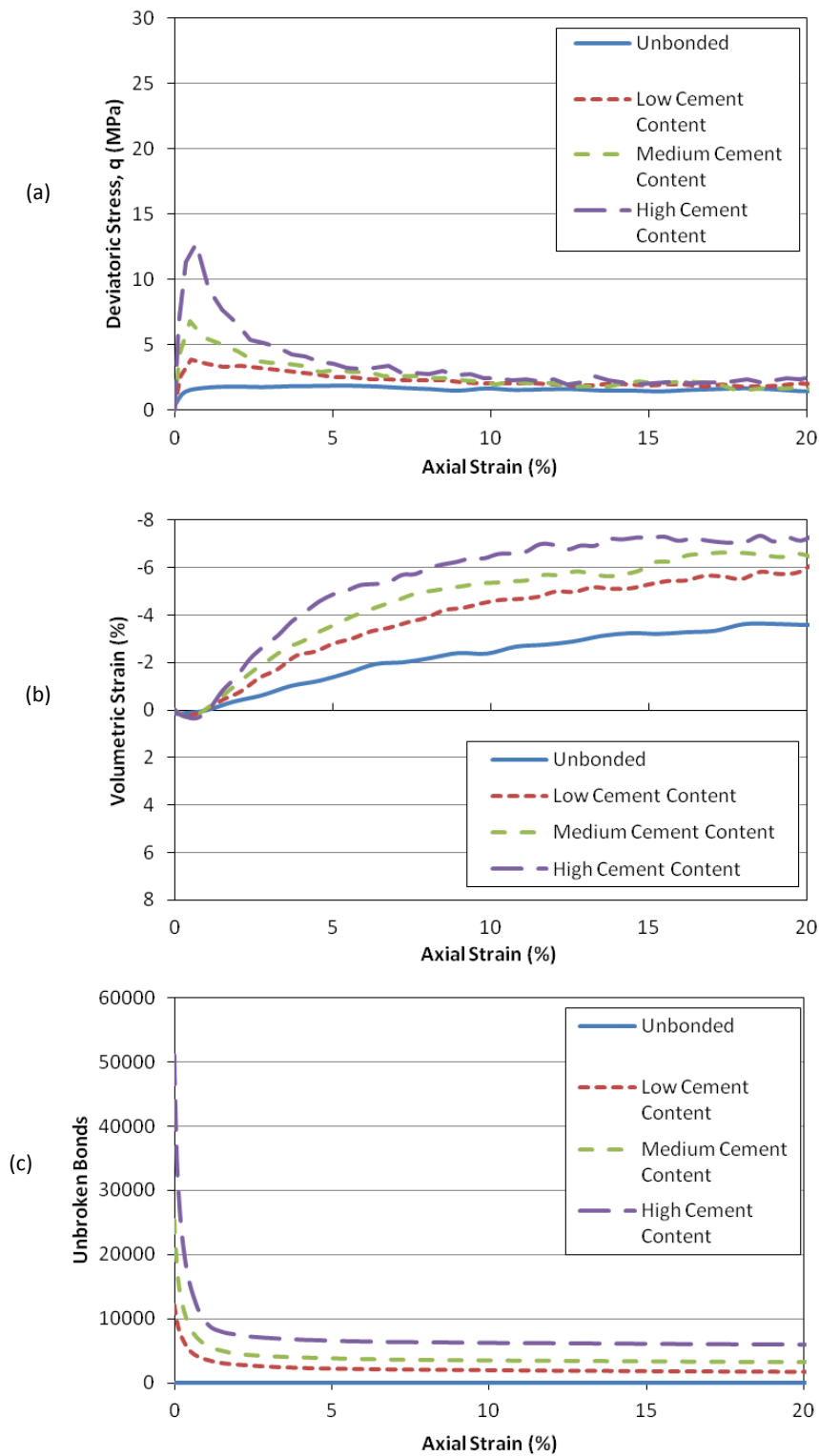


Figure 8. Triaxial results for simulations with various number of bonds representing increasing cement content: deviatoric stress (a), volumetric strain (b) and remaining unbroken bonds (c) versus axial strain

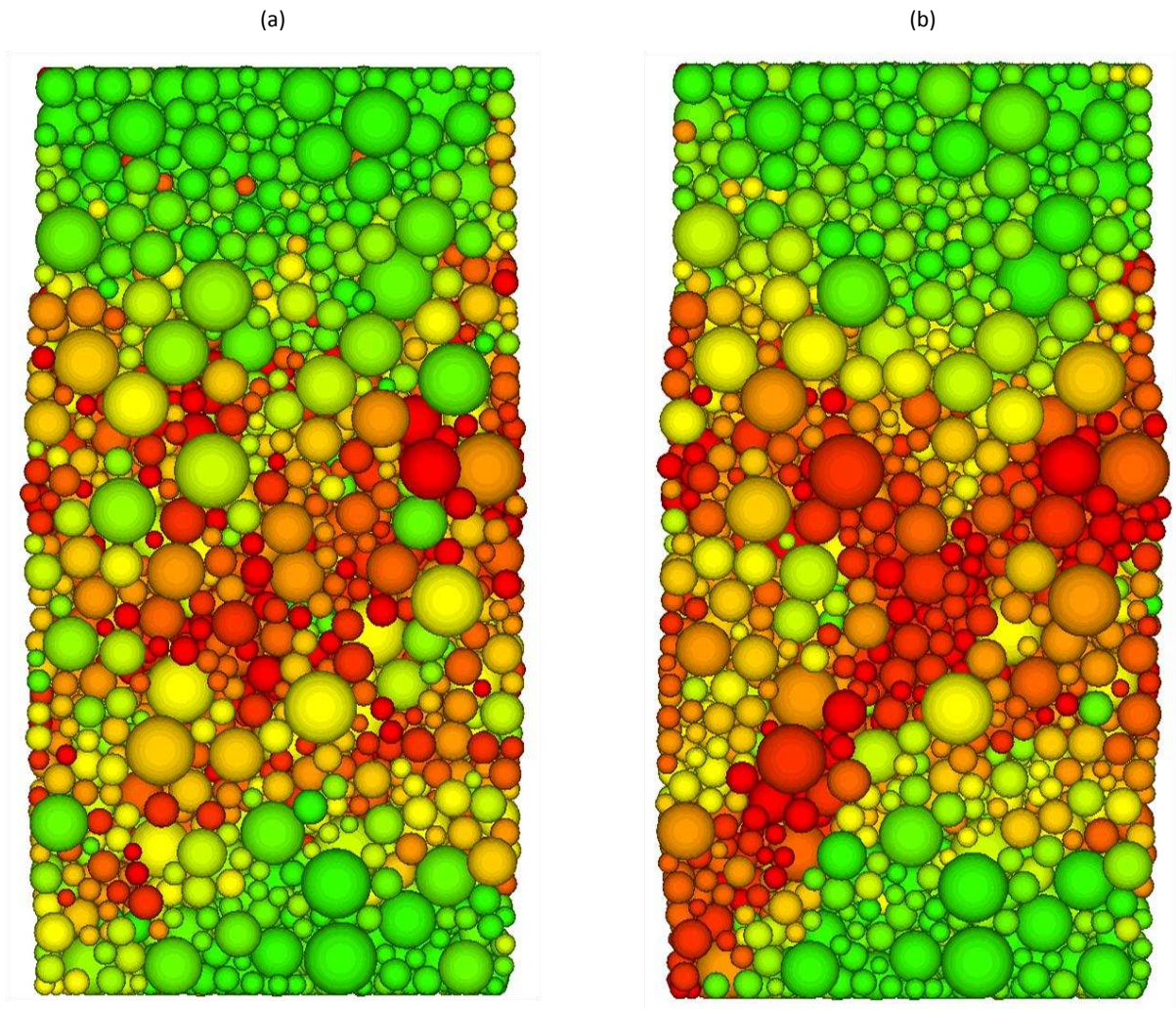


Figure 9. Particle rotations on a vertical plane through the centre of the specimens, after 2-3% axial strain: (a) lightly cemented sample and (b) heavily cemented sample sheared under 1MPa confining pressure. Red denotes the highest rotation

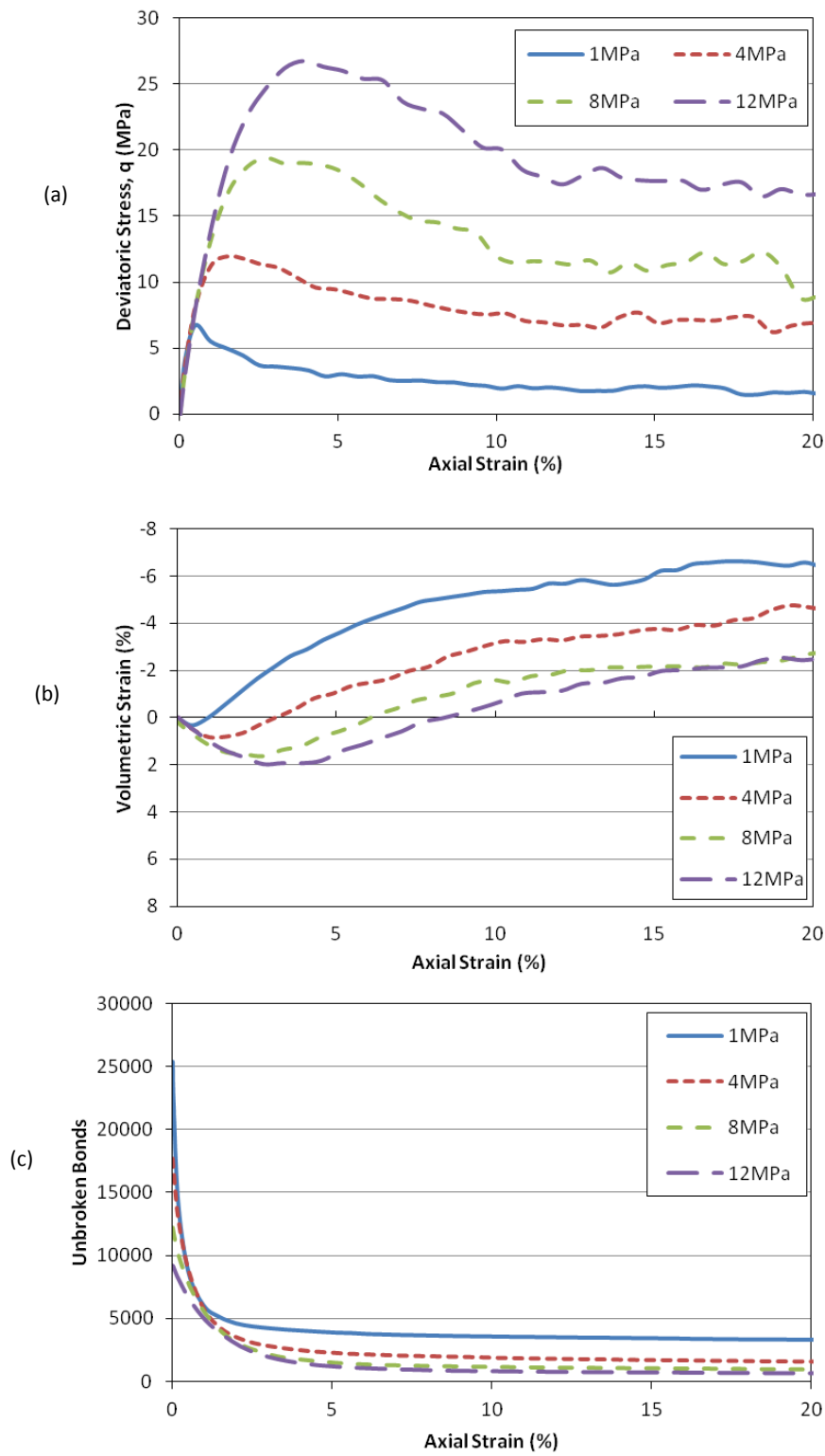


Figure 10. Triaxial Behaviour of a moderately cemented sample (average of 10 bonds per particle) sheared across a range of high confining pressures (1-12MPa): (a) deviatoric stress, (b) volumetric strain and (c) remaining unbroken bonds versus axial strain

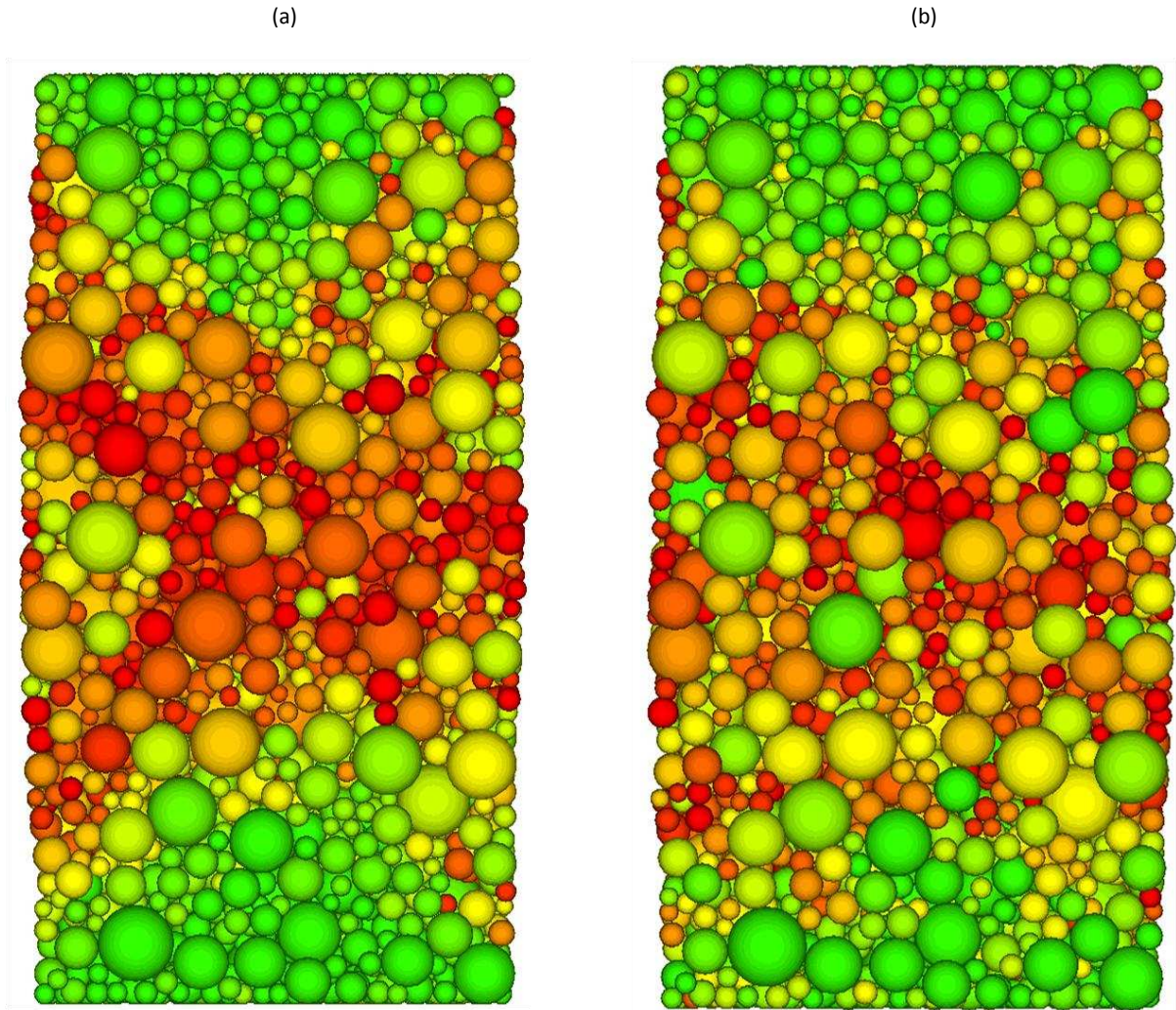


Figure 11. Particle rotations on a vertical plane through the centre of moderately cemented specimens (average of 10 bonds per particle), after 2-6% axial strain: 1MPa confining pressure (a) and 12MPa confining pressure (b). Red denotes the highest rotation



(a)



(b)



**Figure 12. Images of numerical (top) and laboratory (bottom; Marri et al., 2012) cemented specimens after shearing to 20% axial strain under 1MPa (a) and 12MPa (b)**